Research Square

Preprints are preliminary reports that have not undergone peer review.
They should not be considered conclusive, used to inform clinical practice,
or referenced by the media as validated information.

Integration of metabolomics and transcriptomics reveals the therapeutic mechanism underlying Chelidonium majus L. in the treatment of allergic asthma

Renguang Wang
Changchun University of Chinese Medicine
Xintong Sui
Changchun University of Chinese Medicine
Xin Dong
Changchun University of Chinese Medicine
Liming Hu
Changchun University of Chinese Medicine
Zhimeng Li
Changchun University of Chinese Medicine
Hang Yu
Changchun University of Chinese Medicine
Cuicui Li
Changchun University of Chinese Medicine
Guoxin Ji
Changchun University of Chinese Medicine
shumin Wang
wangsm@ccucm.edu.cn
Changchun University of Chinese Medicine

Research Article

Keywords: Chelidonium majus L., allergic asthma, metabolomics, transcriptomics, energy metabolism, inflammation

Posted Date: July 28th, 2023

DOI: https://doi.org/10.21203/rs.3.rs-3147231/v1

License: This work is licensed under a Creative Commons Attribution 4.0 International License.
Read Full License

Version of Record: A version of this preprint was published at Chinese Medicine on April 26th, 2024. See the published version at https://doi.org/10.1186/s13020-024-00932-y.

Abstract

Background

Chelidonium majus L. (*C*. majus) belongs to the Papaveridae family and is the dried whole grass of *C*. majus. It is usually used in clinical practice of traditional Chinese medicine and has been reported of the effect in relieving cough and asthma. However, the mechanism of action is still unknown. This research aimed to illuminate the therapeutic effect of *C*. majus in the inhibition of allergic asthma.

Methods

Asthmatic SD rats were first sensitized and established through ovalbumin (OVA) motivation. Subsequently, lung histopathological analysis (HE, Masson, PAS) and inflammatory cytokines assay (IL-4, IL-17, IL-6) were implemented to evaluate the protective effects of *C*. majus on asthma. Then, the effects of *C*. majus and their molecular mechanisms of action on asthma were detected based on the integration of transcriptomics and metabolomics analyses.

Results

After administration with *C*. majus, the histological injury of inflammation, collagen deposition and mucus secretion in lungs were attenuated and the serum inflammatory cytokines perturbations were also converted. Furthermore, integrated analysis revealed that after *C*. majus treatment, 7 different expression genes (DEGs) (Alox15, P4ha1, Pla2g16, Pde3a, Nme1, Entpd8 and Adcy9) and 9 metabolic biomarkers (ADP, Xanthosine, Hypoxanthine, Inosine, prostaglandin E2 (PGE2), prostaglandin F2a (PGF2a), phosphatidylserine, Creatine and LysoPC(10:0)) were discovered to be connected with the enrichment metabolic pathways, including Purine metabolism, Arachidonic acid metabolism, Arginine and proline metabolism and Glycerophospholipid metabolism. The obtained metabolic biomarkers and DEGs are mainly related to energy metabolism and inflammation, and may be potential therapeutic targets.

Conclusion

C. majus relieved OVA-induced asthma in rats by regulating the Alox15, P4ha1, Pla2g16, Pde3a, Nme1, Entpd8 and Adcy9 genes expression to restore the disorders in energy metabolism and inflammation.

Introduction

Asthma represents the long-term inflammatory respiratory disorder related to the combination of hereditary and environmental variables [1]. It is commonly triggered by various allergens and mainly manifested as chronic airway inflammation, airway hyperresponsiveness, and airway remodeling [2–4]. A previous research found that asthma was mainly caused by the imbalanced Th1-to-Th2 cell ratio, which

primarily result in T cell differentiation in Th2. Th2 lymphocytes can produce Th2 cytokines, which recruits multiple inflammatory cells, including neutrophils, eosinophils and macrophages to the lesions, and then induce airway inflammation [5–8]. According to the scientific statistics, there were more than 300 million individuals suffering from asthma in the world [9]. Corticosteroids, β-Agonists and antihistamines have been used as main clinical drugs for the treatment of asthma. However, the deficiency of long term effects and various adverse reactions gradually displayed in the treatment. At the same time, the emergence of drug resistance in patients also limits their use [10, 11]. Therefore, developing drugs with high effectiveness and safety as complementary or alternative medicines is urgent for asthma treatment. Chinese herbal remedies have long been used for treating asthma, and the effect has attracted increasing attention [12, 13]. *C*. majus, a traditional Chinese medicine that analgesia, spasmolysis, relieves coughing and asthma, was first recorded in Salvation Materia Medica and is now in the list of Chinese Pharmacopoeia 14. Due to its remarkable efficacy in clinical practice, *C*. majus is commonly used for treating spasm, cough, bronchitis, asthma, or additional respiratory system disorders [15, 16]. In recent years, broadly biological activities of *C*. majus extracts have been reported, like anti-inflammatory [17], inhibit smooth muscle [18], anti-viral [19], and anti-bacterial [20] activities.

Metabonomics was considered as the "holistic-dynamic-synthesis-analysis" approach, correspond to dynamic Chinese herbal metabolic processes and holistic concept theory in traditional Chinese medicine [21]. According to reports in literature, a metabolic imbalance was linked to the pathogenesis of asthma [22]. Additionally, metabolites changes are considered closely associated with transcription factors [23]. Integrating metabolic and gene expression data is thought to be a novel strategy for displaying the intricate gene and metabolic pathway regulatory networks. For the first time in this research, metabolomics and transcriptomics were incorporated to determine the molecular mechanism of *C*. majus for asthma.

Material and methods

Reagents and materials

Dexamethasone (Dex) was provided by Suicheng Pharmaceutical Co.; Ltd. (Zhengzhou, China). Ovalbumin (OVA) was offered by Shanghai yuanye Bio-Technology Co.; Ltd (Shanghai, China). interleukin (IL)-4 test kit (No. 220805012R), interleukin (IL)-6 test kit (MM-0190R1), interleukin (IL)-10 test kit (MM-0195R1) and interleukin (IL)-17 test kit (No. MM-0088R1) were provided by Jiangsu Meimian industrial Co.; Ltd (Yancheng, China). The PI3K antibody (No. GR3360941-16), Akt antibody (No. ab179463), NF-κB p65 antibody (No. ab16502) were obtained from Abcam Plc (Cambridge, UK), p-NF-κB p65 antibody (No. 4806) was supplied by Cell Signaling Technology (Boston, USA), IKB-α antibody (No. 00095768) was obtained from Affinity Biosciences (Beijing, China).

Preparation of the ethanol extract from C. majus

C. majus (batch number: C19110704) samples were provided by Hebei Renxin Pharmaceutical Co.; Ltd. (Hebei, China), later certified by Prof. Shumin Wang of Changchun University of Chinese Medicine. The *C*.

majus was ground to powder, and put through a filter with a mesh size of 60, after which the precisely weighed powder (400 g) were refluxed twice for a 1-h period with 80% methanol each time. After conflating, filter liquor, was subjected to concentration under reduced pressure, freeze-drying into powders, finally storage at -80℃ for future use.

Ultra-performance liquid chromatography-quadrupole-Executive Orbitrap mass spectrometry (UPLC-Q-Excutive) analysis of C. majus extract

Methanol containing 2-Amino-3-(2-chloro-phenyl)-propionic acid (4 ppm) was used to dissolve the extract of *C.* majus, followed by a filteration with 0.22 μm membrane. And the composition identification was performed by UPLC-Q-Excutive based on literatures [24, 25].

Animal handling

SD male rats (200 ± 20 g), SPF level, supplied by Changchun Yisi Laboratory Animal Technology Co.; Ltd. [Changchun, China, approval number: SCXK(Ji)2018-0007]. The rats were kept within the plastic cages under 22 ± 2℃, 50 ± 10% humidity, and 12-h/12-h light/dark cycle conditions. Each animal experiment was carried out following Guidelines for Animal Experimentation of Changchun University of Chinese Medicine (Jilin, China). Our experimental protocols (protocols No.: 2020345) gained approval from Animal Ethics Committee of our center. Seventy two rats were randomized as 6 groups (n = 8 each), namely, control (Control), model (Model), Dexamethasone (Dex), low/medium/high-dose *C.* majus (CL, CM, CH) groups. Animal model of asthma was established after 7 days of routine feeding. Sensitizing solutions were prepared as follows: 100 mg OVA, 100 mg aluminum hydroxide dissolved into normal saline (1 mL). The rats in each group were intraperitoneal injected of sensitization solution on the 1st and 8th day respectively. Control rats were given injection of 1 mL normal saline in an identical way. Fifteen days after the last sensitization, each group was continuously gavaged for seven days, Dex group was administered with dexamethasone (0.5 mg/kg), normal saline was given to Control and Model groups, three different doses of *C.* majus (0.9, 1.35, 1.8 mg/kg) were given to other groups respectively. The amount of intragastric administration was 10 $mL \cdot kg^{-1} \cdot d^{-1}$, and 30 min after each administration, the rats were challenged for a 30-min period with 1% OVA solution (w/v) within the plexiglass chamber once daily. Likewise, normal saline was given to control rats (Fig. 1A).

Sampling

After the last atomization inhalation, each rat was fasted for a 12-h period and anesthetized with 1% pentobarbital sodium the next day. The serum samples were collected, and the supernatant was subjected to 10-min centrifugation at 3000 $r \cdot min^{-1}$ before being stored at -80℃. A part of lung tissue was used for pathological analysis through fixation within 4% paraformaldehyde, while the rest was used for transcriptomic analysis.

Pulmonary Histopathology

After fixation using 4% paraformaldehyde, lung tissues were subjected to dehydration in ethylic alcohol, paraffin embedding, slicing in 4-μm sections prior to staining using hematoxylin and eosin (HE), Masson's trichrome (Masson) or periodic acid-Schiff (PAS). Inflammation score was analyzed according to previous description [26, 27]. Double-blind method was used to assess inflammation, collagen deposition, goblet cell hyperplasia and mucus hypersecretion.

Serum inflammatory cytokines test

We conducted Enzyme-linked immunosorbent assay (Elisa) for measuring serum IL-6, IL-4, IL-17 contents.

Serum Metabolomic Profiling

Serum sample was separated chromatographically with the Acquit UPLC HSS T3-C18 column (Waters Corp.; Shanghai, China, 100 mm × 2.1 mm, 1.8 μm) by the Acquit I-Class PLUS instrument (Milford, America). Primary and secondary mass spectrometry data were collected using the Waters Xevo G2-XS QTOF high resolution mass spectrometer in Muse mode by adopting acquisition software (MassLynx V4.2, Waters).

Data processing, multivariate analysis and statistical analyses

Progenesis QI software was utilized to process raw data to extract and align peaks or implement additional data processing, with mass deviation and theoretical fragment identification being < 100 ppm. Those compounds detected were later searched based on KEGG, lipid maps and HMDB databases to obtain pathway and classification data. In line with grouping, we determined and compared difference multiples, and used T test to determine significant difference p-value. OPLS-DA modeling was completed using R language package ropls, then model reliability was tested by 200-fold permutation tests. In addition, multiple cross-validation was used to determine model VIP value. As for OPLS-DA model, its difference multiple, *p*-value and VIP value were combined to screen differential metabolites. Hypergeometric distribution test was used to calculate differential metabolites for the enrichment significance of the KEGG pathway.

Transcriptomic analysis

This work collected lung tissues from Control (n = 3), Model (n = 3) and CH (n = 3) groups for RNA sequencing. RNA content and quality were analyzed with NanoDrop 2000 (Thermo Fisher Scientific, Wilmington, DE). Besides, Agilent Bioanalyzer 2100 system (Agilent Technologies, CA, USA) was employed for assessing RNA integrity with RNA Nano 6000 Assay Kit. The cDNA library was constructed and evaluated for quality using Agilent Bioanalyzer 2100 system (Agilent Technologies, Inc.).

RNA sequencing and data analysis

Differential expression was analyzed by DESeq2 R package upon the criteria of $p < 0.05$ and $|\log2(\text{FoldChange})| > 1$. Gene function was annotated based on KO (KEGG Ortholog) databases.

Immunohistochemical (IHC) staining

The lung tissue sections were fixed in, dewaxed to water, subsequently performed with antigen repair. And PI3K, Akt, NF-κB p65, p-NF-κB p65, IKB-α antibodies were used to incubate overnight at 4 ℃ after sealing with 3% BSA under ambient temperature for a 30-min period. Corresponding secondary antibody was added for incubation under ambient temperature for 50 min. An optical microscope was utilized to observe slices. Intensities were quantified with Image Pro Plus 6.0 software. Three separate fields from each section and five tissue samples from each group were assessed.

Establishment of the DEGs-based protein-protein interaction (PPI) network and hub gene analyses

PPI network of Model-vs-Control and CH-vs-Model groups overlapping DEG was constructed based on STRING database, followed by importing in Cytascape 3.9.1 platform for network visualization. In addition, CytoNCA plug-in was adopted for counting node topological parameters within PPI network for further hub gene screening.

Quantitative real-time PCR (qRT-PCR) analysis

The hub genes were verified by qRT-PCR. By adopting Trizol reagent, we isolated total tissue RNA in line with commercial protocols. Later, through using SYBR Green Premix Ex TaqII, mRNA levels were detected with β-actin being the amplification reference. The final data were analyzed through $2^{-\triangle\triangle Ct}$ approach, and primer sequences can be seen from Table 1.

Table 1
The primer of hub genes.

gene	Former Primer	Reverse Primer
IL6	GAGTTGTGCAATGGCAATTCTG	ACGGAACTCCAGAAGACCAGAG
IL10	AGAAGCTGAAGACCCTCTGGATA	TTCATTTTGAGTGTCACGTAGGC
H3f3c	TTCAAAACAGACCTGCGCTTC	ATGGATAGCACACAGGTTGGTATCT
Cdk1	GAAAGCGAGGAAGAAGGAGTGC	CTGCCAGTTTGATTGTTCCTTTGT
Cxcl2	CTGTACTGGTCCTGCTCCTCCT	AGTGGCTATGACTTCTGTCTGGG
Aurkb	CATCCCTGAGGAGGAAGACCAT	TGCTCCAGAGGCAGTCGTTGT

Integrating transcriptomics and metabolomics analyses

The present work used MetaboAnalyst 5.0 for integrating transcriptomics and metabolomics data for acquiring a comprehensive relevance between the DEGs and metabolic biomarkers. The qRT-PCR was applied to testify the 10 key genes based on the method expressed before. The sequences of primers were shown in Table 2.

Table 2
The primer of key genes.

gene	Former Primer	Reverse Primer
Nme1	ACTACATTGACCTGAAGGACCGC	CCTGTCTTCACAACATTCAGTCCC
Pla2g16	GATATGTGATCCACCTGGCTCC	GTTCAGAGGCAGCGGAGTGTA
Entpd8	TCCCTGAACTACACCCAGAACCT	CATAGAACTGGCCATGCACG
Alox15	TGCTTCTATGCTAAAGACGCCC	GCCAAGATGGACGGAAGAGT
Pde3a	CAGCATAAAGCCACATGAAGCC	ACAGCATAGGACGAAGTGAAGGAC
Rrm2b	TTTCAGTACCTGGTAAACAAGCC	ATGACTGCAAATCGCTGATACTC
Pde7b	GGCTCCTACCCGTTCATTGACT	GTCCAAGGTAGTCTTCGTCCAGC
P4ha1	AGATCCAGAAGGGTTTGTCGG	CAACCTGGTCTTCGTCGTTAGG
Adcy9	TGAGACCTTCGGTTACCATTTCC	GACCTCACCTGAGACATGACAAAC
Ptgs2	CTGATGACTGCCCAACTCCC	CTGGGCAAAGAATGCGAACA

Statistical analysis

Graphpad prism 8 was employed for analyzing pharmacodynamic profiles. Results were represented by mean ± SEM ($\bar{x} \pm s$). Inter-group differences were evaluated by one-way ANOVA, where $p < 0.05$ and $p < 0.01$ indicated statistical significance.

Results

Chemical analysis of C. majus extract

C. majus extract was analyzed by UPLC-Q-Excutive (Fig. 1B). 19 compounds were identified under positive ion mode, including Magnocurarine, Magnoflorine, Chelamine, Protopine, Allocryptopine, Chelidonine, (S)-N-Methylstylopine, Tetrahydrocoptisine, Coptisine, Homochelidonine, Norchelidonine, Sanguinarine, Berberine, Chelerythrine, Chelilutine, Oxysanguinarine, 6-Methoxydihydrosanguinarine, Dihydrochelerythrine, Corysamine. Supplementary Table S1 showed the detailed information with retention time, molecular formula, MS fragment of these compounds.

Roles of C. majus exposure in OVA-mediated changes of body weight and relative lung weight in rats.

There was no obvious variation of initial body weight or relative lung weight among the rats of 6 groups. Compared to Control group rats, OVA challenge lead to an evident reduction ($p < 0.01$) of body weight whereas a remarkable increase ($p < 0.01$) of relative lung weight in Model group rats. Administration with dexamethasone, medium and high dose of *C.* majus displayed a remarkable elevation in body weight ($p <$

0.05) whereas suppression ($p < 0.01$, $p < 0.05$, $p < 0.01$) in relative lung weight when compared to Model group rats (Fig. 1C, D).

Figure 1 (A) Experimental scheme. (B) Total ion chromatograms (+) of *C.* majus extract. (C, D) Body weights and relative lung weights of diverse groups after administration.

C. majus reduced inflammation, collagen deposition and mucus hypersecretion in OVA-induced asthmatic rats

Control group did not show abnormal findings of the structure in the bronchial and alveolar. Nevertheless, model rats showed an obviously increased thickness in the alveolar septum, and tremendous inflammatory cell infiltrations in bronchi and perivascular. Intragastric administration of Dex, medium and high dose of *C.* majus all apparently alleviated the severity of pulmonary lesion compared with Model group ($p < 0.01$, $p < 0.05$, $p < 0.01$). (Fig. 2A, D). As revealed by Masson staining, the collagen deposition of Model group was severe. Administration with Dex and high dose of *C.* majus both markedly alleviated the collagen deposition in OVA-induced rats ($p < 0.01$) (Fig. 2B, E). Based on PAS staining, there was no visible edema on the airway mucosa in Control group, and few goblet cells, little mucus secretion can be seen. On the contrary, lungs tissue structure of Model group were irregular with obvious edema on the airway mucous membrane, and massive goblet cells proliferate on airway epithelium, and the mucus hypersecretion can be seen in the inner wall of airway. And the goblet cell proliferation and mucus secretion were attenuated in Dex, CH groups rats ($p < 0.01$). (Fig. 2C, F). The results indicated that high dose of *C.* majus obviously attenuated the pulmonary histopathology of asthmatic rats.

C. majus regulate inflammatory cytokines production within asthmatic rats

According to statistical analyses, Model group had evidently increased IL-4, IL-6, and IL-17 levels ($p < 0.01$) relative to Control group. Inversely, in comparison with Model group, IL-17 and IL-4 expression reduced obviously ($p < 0.01$), IL-6 expression reduced obviously ($p < 0.01$, $p < 0.05$) in Dex and CH groups, administration with medium dose of *C.* majus showed a remarkable decrease in the level of IL-17, IL-4 ($p < 0.05$). (Fig. 2G-I). These findings demonstrated that *C.* majus exhibited good performance in anti-inflammatory effect, and the high dose was more effective than medium dose.

Figure 2 Pulmonary histopathology analysis. (A) H&E analysis (×200), blue arrows indicate inflammatory cell infiltration. (B) Masson analysis (×200). (C) PAS analysis of pulmonary sections (×200), red arrows indicate goblet cell proliferation. (D) inflammation score. (E) Masson score. (F) PAS score. The data are represented by mean ± SEM (n = 3). ##$p < 0.01$ versus Control group; *$p < 0.05$, **$p < 0.01$ versus Model group. (G-I) Inflammatory cytokines assay. The data are represented by mean ± SEM (n = 8). ##$p < 0.01$ versus Control group; *$p < 0.05$, **$p < 0.01$ versus Model group.

Metabolomic analysis

Control group was significantly separated from Model group, CH group was basically separated from Model group and approached Control group, based on PCA score plots (Fig. 3A). According to these results, there were significant differences in metabolite profiles of CH groups relative to Model group, and CH group manifested a better performance of the recovery from OVA-induced metabolic disturbance. The parameters R2Y, Q2 values of OPLS-DA were approached to 1 (0.99 and 0.91), which implied the presence of less unrelated variables of OPLS-DA models. For checking reliability of OPLS-DA model, replacement tests were carried out. R2 and Q2 values remarkably decreased compared with original points, which was indicative of the asthma model being well built (Fig. 3B-E). According to the multivariate analysis of OPLS-DA with the parameters settings of FC > 1, VIP > 1 and $p < 0.05$, we detected 46 candidate serum metabolites to be metabolic biomarkers that mainly associated with lipid, organic acid, fatty acid, and amino acid. Compared with Control group, 15 metabolites in Model group showed up-regulated, whereas 31 showed down-regulated. When compared with Model group, 12 metabolites of CH group were down-regulated, 18 metabolites were up-regulated (Supplementary Table S2). The metabolite heatmap is shown in Fig. 3F.

MetaboAnalyst 5.0 was used to analyze pathways of all metabolic biomarkers with the filter Criteria of -log P > 1 and Impact > 0. 11 main metabolic pathways were determined in Control and Model group, included Arginine and proline metabolism, Citrate cycle, Pyruvate metabolism, Purine metabolism, Arachidonic acid metabolism, Arginine biosynthesis, Tyrosine metabolism, Sphingolipid metabolism, beta-Alanine metabolism, Phenylalanine, Tyrosine and tryptophan biosynthesis and Alanine, aspartate and glutamate metabolism. 6 major metabolic pathways could be detected from CH and Model group, included Arginine and proline metabolism, Arginine biosynthesis, Purine metabolism, beta-Alanine metabolism, Glycerophospholipid metabolism, and Phenylalanine, tyrosine and tryptophan biosynthesis (Fig. 3G, H).

To sum up, asthma induction disturbed these metabolic biomarkers as well as the associated metabolic pathways. The alteration was mainly associated with lipid, amino acid, and fatty acids metabolic disorders. Following intervention with high dose of *C.* majus, the disorder was restored to some extent.

Figure 3 Metabolomic results. (A) PCA score plots. (B-E) OPLS-DA score plots. (F) Heatmap visualization for metabolic biomarkers in Control, Model and CH groups (n = 6). (G, H) Metabolic pathway analysis of Model-vs-Control group, Model-vs-Control group and CH-vs-Model groups.

Transcriptomics analysis

KEGG enrichment analysis

There were altogether 754 DEGs detected when comparing Model-vs-Control group, including 454 with up-regulation while 300 with down-regulation. After treatment, there were 260 DEGs regulated in CH group, including 165 showing up-regulation whereas 95 showing down-regulation relative to Model group (Fig. 4A). Heatmap was obtained by clustering the DEGs (Fig. 4B). Supplementary Table S3 displays details for the DEGs. After high dose of *C.* majus intervention, gene levels within lung tissue showed a

similarity to Control group, indicating the role of *C.* majus in regulating DEGs levels in Model group. In order to investigate DEGs-regulated biological pathways, we carried out KEGG analysis. Figure 4C, D displayed the 20 most significant pathways. Those pathways enriched were chiefly related to inflammatory pathways (Cytokine-cytokine receptor interaction, Chemokine pathway, IL-17 pathway, TNF pathway, PI3K-Akt pathway, T17 cell differentiation pathway), immune pathways (Intestinal immune network for IgA production pathway, Hematopoietic cell lineage pathway), airway remodeling related signaling pathway (ECM-receptor interaction pathway), energy metabolism pathway (Purine metabolism pathway) and Asthma pathway of Model-vs-Control group. The enrichment pathways were mostly related to inflammation signaling pathways (IL-17 pathway, Cytokine-cytokine receptor interaction, NF-κB pathways, PI3K-Akt pathway, TNF pathway, Chemokine pathway, NOD-like receptor pathway, Arachidonic acid metabolism), energy metabolism pathways (Purine metabolism), airway remodeling related signaling pathway (ECM-receptor interaction pathway) and Pertussis of Model-vs-Control and CH-vs-Model groups.

Figure 4 Transcriptomics results (n = 3). (A) Venn diagram showing DEGs in different groups. (B) Heatmap showing DEGs in Control, Model and CH groups. (C, D) KEGG pathway enrichment on DEGs-Bubble chart of Model-vs-Control group and Model-vs-Control and CH-vs-Model groups respectively.

We selected PI3K-Akt and NF-κB pathways for verifying the roles of *C.* majus in resisting inflammation when treating asthma. Compared with Control group, PI3K, Akt, NF-κB p65, p-NF-κB p65 levels had up-regulated significantly ($p < 0.01$, $p < 0.01$, $p < 0.05$, $p < 0.01$), while IKB-α level had down-regulated significantly ($p < 0.05$) of Model group. After high dose of *C.* majus administration, PI3K, Akt, NF-κB p65, p-NF-κB p65 levels had down-regulated dramatically ($p < 0.05$), IKB-α level had up-regulated evidently ($p < 0.05$) relative to Model group (Fig. 5A, B).

PPI network establishment and hub gene analyses

Based on these findings, 260 shared DEGs of Model-vs-Control and CH-vs-Model groups were obtained. PPI networks were built through STRING database, followed by visualization with Cytoscape 3.9.1 platform (Fig. 5C). And then according to degree centrality, 6 genes showing the greatest degree values were acquired, including Il-6 (degree = 60), Il-10 (degree = 48), H3f3c (degree = 30), Cdk1 (degree = 28), Cxcl2 (degree = 26) and Aurkb (degree = 26) of Model-vs-Control and CH-vs-Model groups.

For validating functions of *C.* majus in asthma by those potential hub genes, Il-6, IL-10, H3f3c, Cdk1, Cxcl2 and Aurkb mRNA expression was detected through qRT-PCR. According to Fig. 5D, OVA-induced asthma caused an obvious upregulation of Il-6, H3f3c, Cdk1, Cxcl2 and Aurkb ($p < 0.05$, $p < 0.01$, $p < 0.05$, $p < 0.01$, $p < 0.01$) relative to Control group. Administration with high dose of *C.* majus induced a significant down-regulation of Il-6, Cdk1, H3f3c, Cxcl2, Aurkb ($p < 0.05$). Unluckily, IL-10 was not detected.

Figure 5 (A, B) IHC detection of PI3K, Akt, IKB-α, NF-κB p65, p-NF-κB p65 protein levels within rats lung tissues. The data is represented by mean ± SEM (n = 3). #$p < 0.05$, ##$p < 0.01$ versus Control group; *$p < 0.05$ versus Model group. (C) PPI networks regarding DEGs in Model-vs-Control and CH-vs-Model groups.

(D) hub genes verification. Results are represented by mean ± SEM (n = 3). #$p < 0.05$, ##$p < 0.01$ versus Control group; *$p < 0.05$, **$p < 0.01$ versus Model group.

Integration of metabolomics and transcriptomics analyses

The linked network of metabolic biomarkers and DEGs was displayed in Figure. 6A with the filter Criteria of -log P > 1, mainly included Arginine and proline metabolism, Arginine biosynthesis, Glycerophospholipid metabolism, Citrate cycle (TCA cycle), Pyruvate metabolism, Arachidonic acid metabolism, Purine metabolism, Tyrosine metabolism, Sphingolipid metabolism, beta-Alanine metabolism, Phenylalanine, tyrosine and tryptophan biosynthesis in Model-vs-Control group and Purine metabolism, Arachidonic acid metabolism, Retinol metabolism, Arginine and proline metabolism, Aminoacyl-tRNA biosynthesis, Glycerophospholipid metabolism, Linoleic acid metabolism, Ether lipid metabolism, Pyrimidine metabolism, Pyruvate metabolism in both Model-vs-Control and CH-vs-Model groups.

The metabolic biomarkers and DEGs were analyzed using spearman rank correlation (Fig. 6B and C). As was shown, there was noticeable correlation between some metabolites and DEGs. Pde3a, Adcy9 were negatively related with ADP, Inosine ($p < 0.01$), Xanthosine ($p < 0.05$), Hypoxanthine ($p < 0.05$, $p < 0.01$). Pde7b was negatively related with ADP, Inosine, Xanthosine ($p < 0.01$, $p < 0.05$, $p < 0.05$) and Entpd8 was positively related with ADP, Inosine, Xanthosine, Hypoxanthine ($p < 0.01$, $p < 0.01$, $p < 0.05$, $p < 0.05$). Rrm2b was positively related with ADP ($p < 0.05$), Xanthosine ($p < 0.01$), and negatively related with Inosine ($p < 0.01$). Nme1 was positively related with ADP and Inosine ($p < 0.05$). Pla2g16 was positively interrelated with PGE2 and phosphatidylserine ($p < 0.05$, $p < 0.01$) and negatively interrelated with LysoPC(10:0) ($p < 0.05$). Alox15 was negatively interrelated with PGF2a ($p < 0.05$). Ptgs2 was positively interrelated with PGF2a ($p < 0.05$). P4ha1 was negatively associated with Creatine (10:0) ($p < 0.01$). The results supplied a reference for the mechanism of alleviating asthma by *C.* majus.

Furthermore, to evaluate our results, qRT-PCR was carried out for verifying mRNA levels of those 10 genes (Fig. 6D). As a result, relative to Control group, Ptgs2, Entpd8, Pla2g16 and Nme1 levels within lung tissues in Model group rats had markedly elevated ($p < 0.05$, $p < 0.01$, $p < 0.01$, $p < 0.05$), Adcy9, Alox15, P4ha1, Pde3a and Pde7b levels were notably reduced ($p < 0.05$, $p < 0.01$, $p < 0.05$, $p < 0.05$, $p < 0.05$), but Rrm2b didn't change. Relative to Model group, administration with high dose of *C.* majus suppressed Entpd8, Pla2g16 and Nme1 levels within lung tissues ($p < 0.01$), while facilitated Adcy9, Alox15 and P4ha1 levels ($p < 0.01$), but Pde7b and Ptgs2 levels remained unchanged.

The associated DEGs and metabolic biomarkers were displayed in Fig. 6E. 7 DEGs (Alox15, P4ha1, Pla2g16, Pde3a, Nme1, Entpd8 and Adcy9) were discovered related to the enrichment metabolic pathways. P4ha1 was related to Arginine and proline metabolism. Alox15 was associated with Arachidonic acid metabolism, Pla2g16 participated in Glycerophospholipid metabolism, Pde3a, Nme1, Entpd8 and Adcy9 were involved with Purine metabolism.

Figure 6 (A) Joint-Pathway analysis of Model-vs-Control and CH-vs-Model groups. (B, C) Correlation analysis between metabolic biomarkers and DEGs on the basis of spearman rank. (D) qRT-PCR validation of the 10 genes. Results are represented by mean ± SEM (n = 3). #$p < 0.05$, ##$p < 0.01$ versus Control group; *$p < 0.05$, **$p < 0.01$ versus Model group. (E) Changes in metabolites (blue squares) and differential genes (red circles) in the 4 metabolism on the basis of integrated analysis. The red arrow indicates the increase or decrease of Model group relative to Control group. The green arrow reveals the increase or decrease of CH relative to Model group.

Discussion

Cumulative evidence suggested that chronic airway inflammation is the key to the pathogenesis, and is also the basis of airway hyperreactivity and airway remodeling [28]. The inflammatory responses are induced by production of various inflammatory factors, such as IL-4, IL6, IL17 that are mediated by Th2 cells [6, 7]. The Elisa assay showed that *C*. majus could reduce levels IL-4, IL-6, IL-17. Besides, such decreased inflammation scores that caused by *C*. majus were also observed through HE analysis, indicating that *C*. majus may suppress inflammmation through regulating Th2 inflammatory factors levels.

Recently, PI3K/Akt/NF-κB signal pathway has been found intimately related to activation and immune responses of T and Blymphocytes, eosinophils and mast cells in the development of asthma [29–31]. As a transcriptional regulator, nuclear factor (NF)-κB plays an important role in asthma inflammatory pathway. PI3K/Akt can activate the inhibitory protein kinase of NF-κB while accelerating IκB degradation, which contribute to uclear translocation as well as transcriptional activity of NF-κB [32]. The IHC analysis suggested *C*. majus attenuated asthma through restraining PI3K/Akt/NF-κB pathway.

Collagen is a type of extracellular matrix protein, and its deposition on the airway wall signifies the occurrence of airway remodeling [33]. One of the hallmarks of asthma is mucus overproduction from goblet cells [34]. Masson analysis showed that high dose of *C*. majus inhibited collagen deposition to improve airway remodeling. PAS and the relative weight of lungs analysis demonstrated that high dose of *C*. majus suppressed the goblet cell proliferation and mucus secretion.

In this study, a prominent metabolic and transcriptional feature observed in asthmatic rats was an alteration to cellular energy metabolism and the expression of related genes in lungs, possibly involved in an increased respiratory burden in providing energy to recruited inflammatory cells. Pde3a, Entpd8, Nme1 and Adcy9 took part in the process of ATP transformation. After administration with high dose of *C*. majus, the levels of Nme1, Entpd8 expression and Xanthosine, Hypoxanthine, Inosine, ADP decreased, the levels of Pde3a, Adcy9 expression increased, indicating that *C*. majus reversed the disorders of energy metabolism.

Besides, various inflammatory cells and inflammatory mediators are active throughout the entire pathogenic course of asthma. Local inflammation is also related with tissue hypoxia due to a integration of reduced and oxygen supply and elevated oxygen requirement of resident and infiltrating cells as a

result of the inflammatory response [35]. As was reported that there was a high expression of Alox15 in airway epithelial cells where arachidonic acid was convered to 15-hydroxyeicosatetraenoic acid by Alox15 [36]. PGE2 has been proved to aggravate several inflammatory responses and immune diseases, and PGF2a has been relevant to the acute and chronic inflammation [37–39]. Ptgs2 served as the key enzyme in the biosynthesis of prostaglandin. Phosphatidylserine was investigated to play a vital role in Th2-induced airway hyperreactivity and was closely related with inflammatory cells like eosinophils and macrophages [40]. In this reserch of Model group rats, PGE2, PGF2a, phosphatidylserine and Ptgs2 levels elevated, Alox15 level reduced, which possibly aggravated airway inflammation and airway hyperreactivity. Following high dose of *C*. majus treatment, they all showed obvious reverse levels except for Ptgs2, and further investigation needs to be conduct for the reason.

Inosine is related to tissue damage, hypoxia and inflammation [41]. The increased inosine expression indicated that the asthmatic rats body may be under anoxic conditions and associated with inflammation. As shown in previous researches, Creatine is engaged in energy supply of smooth muscles, and a significant increase in creatine was observed in inflamed lungs [42]. LysoPCs have been reported to be reduced in asthmatic rats and may served as immune suppressors [43]. In this reserch, LysoPC(10:0) displayed reduced level, Creatine and Inosine exhibited increased levels in Model group. The abnormal alteration in Glycerophospholipid metabolism and Arginine and proline metabolism might contributed to inflammation and energy disorder. After treatment with high dose of *C*. majus, they all recovered to normal levels.

Conclusion

Our current findings demonstrated that *C*. majus exerted therapeutic effect on airway inflammation, mucus hypersecretion and airway remodeling of OVA-induced asthma. Correlated analysis of transcriptomics and metabolomics studies indicate that 7 DEGs (Alox15, P4ha1, Pla2g16, Pde3a, Nme1, Entpd8 and Adcy9) and 9 metabolic biomarkers (ADP, Xanthosine, Hypoxanthine, Inosine, PGE2, PGF2a, phosphatidylserine, Creatine and LysoPC(10:0)) were involved in the enrichment metabolic pathways of Purine metabolism, Arachidonic acid metabolism, Arginine and proline metabolism and Glycerophospholipid metabolism. And high dose of *C*. majus may alleviate asthma through impacting on energy metabolism and inflammation. Our study provided a new insight of the therapeutic mechanism for the treatment of asthma by *C*. majus, which contributes to the pharmacological research and further clinical application of *C*. majus.

Abbreviations

C. majus: *Chelidonium majus* L.; Dex: Dexamethasone; Elisa: Enzyme-linked immunosorbent assay; HE: hematoxylin and eosin; KEGG: kyoto encyclopedia of genes and genomes; IL: Interleukin; PPI: producer price index; Masson: Masson's trichrome; OVA: Ovalbumin; PGs: prostaglandins; PAS: periodic acid-Schiff; PCA: principal components analysis; PGE2: prostaglandin E2; PGF2a: prostaglandin F2a; qRT-PCR: quantitative reverse transcription-polymerase chain reaction; UPLC-Q-Excutive Orbitrap/MS: ultra-

performance liquid chromatography-quadrupole-Executive Orbitrap mass spectrometry; VIP: variable importance in projection; OPLS-DA: supervised orthogonal partial least squares discriminant; DEGs: different expression genes; LysoPC: lysophosphatidylcholine.

Declarations

Acknowledgements

Not applicable.

Authors' contributions

SMW designed the research. RGW assisted with data curation, writing-original draft. XTS assisted with writing-review. LMH participated in project administration, editing and funding acquisition. XD and ZML performed investigation, methodology and software. HY, GXJ and CCL performed supervision, formal analysis, conceptualization and resources. Our authors agreed to final version for publication.

Funding

This work was supported by the Jilin Scientific and Technological Development Program of China (No. 192485YY010358427).

Availability of data and materials

The datasets used and/or analyzed during the current study are available from the corresponding author on reasonable request.

Declarations Ethics approval and consent to participate

The experiments using nude mice were approved by institutional guidelines for the care and use of laboratory animals approved by the Animal Care and Use Committee of Changchun University of Chinese Medicine.

Consent for publication

Not applicable.

Competing interests

Our authors claimed no competing interests.

Author details

[1]College of pharmacy, Changchun University of Chinese Medicine, Changchun 130117, China.

[2]Jilin Zhong Ke Bio-engineering Co. Ltd., Changchun 130012, China

References

1. Krusche J, Twardziok M, Rehbach K, Böck A, Tsang MS, Schröder PC, Kumbrink J, Kirchner T, Xing Y, Riedler J, Dalphin J-C, Pekkanen J, Lauener R, Roponen M, Li J, Wong CK, Wong GWK, Schaub B, Ege M, Depner M, Illi S, Loss GJ, Renz H, Pfefferle PI, Kabesch M, Genuneit J, Karvonen AM, Hyvärinen A, Kirjavainen PV, Remes S, Braun-Fahrländer C, Roduit C, Frei R, Kaulek V, Dalphin M-L, Divaret-Chauveau A, Doekes G. TNF-α–induced protein 3 is a key player in childhood asthmadevelopment and environment-mediated protection. J N A Clinical Immunol. 2019;144(6):1684–96. .e12.https://doi.org./10.1016/j.jaci.2019.07.029.
2. Bulani V, Biyani K, Kale R, Joshi U, Pagor R. Inhibitory effect of calotropis giganteaextract on ovalbumin-induced airway inflammation and arachidonic acid induced inflammation in a murine model of asthma. Int J Cur Bio Med Sci. 2011;257–69. https://doi.org./10.1016/j.fct.2009.02.022.
3. Gillissen A, Paparoupa M. Inflammation and infections in asthma. Clin Respir J. 2015;9(3):257–. 10.1111/crj.12135. 69.https://doi.org./.
4. Zhang Y, Jing Y, Qiao J, Luan B, Wang X, Wang L, Song Z. Activation of the mTOR signaling pathway is required for asthma onset. Sci Rep. 2017;7(1):4532. https://doi.org./10.1038/s41598-017-04826-y.
5. Corren J. Role of interleukin-13 in asthma. Curr Allergy Asthma Rep. 2013;13(5):415–. 10.1007/s11882-013-0373-9. 20.https://doi.org./.
6. Ling H, Fabbri M, Calin GA. MicroRNAs and other non-coding RNAs as targets for anticancer drug development. Nat Rev Drug Discov. 2013;12(11):847–65. https://doi.org./10.1038/nrd4140.
7. Erle DJ, Sheppard D. The cell biology of asthma. J Cell Biol. 2014;205(5):621–. 10.1083/jcb.201401050. 31.https://doi.org./.
8. Fahy JV. Type 2 inflammation in asthma-present in most, absent in many. Nat Reviews Immuno. 2014;15(1):57–65. https://doi.org./10.1038/nri3786.
9. Mukherjee AA, Kandhare AD, Rojatkar SR, Bodhankar SL. Ameliorative effects of Artemisia pallens in a murine model of ovalbumin-induced allergic asthma via modulation of biochemical perturbations. Biomed Pharmacother. 2017;94:880–9. .https://doi.org./10.1016/j.biopha.2017.08.017.
10. Reinhold T, Lindig C, Willich SN, Brüggenjürgen B. Patient characteristics in German allergological practices-a nationwide survey. Allergologie Sel. 2018;2(1):39–48. https://doi.org./10.5414/alx01348e.
11. Chapoval SP, García LN, Leimgruber C, Nicola JP, Quintar AA, Maldonado CA. Neonatal endotoxin stimulation is associated with a long-term bronchiolar epithelial expression of innate immune and anti-allergic markers that attenuates the allergic response. PloS One. 2020;15(5):e0226233. https://doi.org./10.1371/journal.pone.0226233.
12. Ji W, Zhang Q, Shi H, Dong R, Ge D, Du X, Ren B, Wang X, Wang Q. The mediatory role of Majie cataplasm on inflammation of allergic asthma through transcription factors related to Th1 and Th2.

Chin. Med. 2020;24(15):53. https://doi.org./10.1186/s13020-020-00334-w.

13. Hsu WH, Lin LJ, Lu CK, Kao ST, Lin YL. Effect of You-Gui-Wan on House Dust Mite-Induced Mouse Allergic Asthma via Regulating Amino Acid Metabolic Disorder and Gut Dysbiosis. Biomolecules. 2021;11(6):821. https://doi.org./10.3390/biom11060812.
14. Chinese Pharmacopoeia Commission. Pharmacopoeia of the People's Republic of China. Volume I. Beijing: China Medical Science Press; 2020. p. 292.
15. Gilca M, Gaman L, Panait E, Stoian I, Atanasiu V. Chelidonium majus–an integrative review: traditional knowledge versus modern findings. Forsch Komplementmed. 2010;17(5):241–8. .https://doi.org./10.1159/000321397.
16. Gu Y, Qian D, Duan JA, Wang Z, Guo J, Tang Y, Guo S. Simultaneous determination of seven main alkaloids of Chelidonium majus L. by ultra-performance LC with photodiode-array detection. J Sep Sci. 2010;33(8):1004–9. .https://doi.org./10.1002/jssc.200900690.
17. Park JE, Cuong TD, Hung TM, Lee I, Na M, Kim JC, Ryoo S, Lee JH, Choi JS, Woo MH, Min BS. Alkaloids from Chelidonium majus and their inhibitory effects on LPS-induced NO production in RAW264.7 cells. Bioorg Med Chem Lett. 2011;21(23):6960–3. .https://doi.org./10.1016/j.bmcl.2011.09.128.
18. Kuenzel J, Geisler K, Strahl O, Grundtner P, Beckmann MW, Dittrich R. Chelidonium majus and its effects on uterine contractility in a perfusion model. Eur J Obstet Gynecol Reprod Biol. 2013;169(2):213–7. .https://doi.org./10.1016/j.ejogrb.2013.03.014.
19. Monavari SH, Shahrabadi MS, Keyvani H, Bokharaei-Salim F. Evaluation of in vitro antiviral activity of Chelidonium majus L. against herpes simplex virus type-1. Afr J Microbiol Res. 2012;6(20):4360–4. .https://doi.org./10.5897/AJMR11.1350.
20. Pan J, Yang Y, Zhang R, Yao H, Ge K, Zhang M, Ma L. Enrichment of chelidonine from Chelidonium majus L. using macroporous resin and its antifungal activity. J Chromatogr B. 2017;1070:7–14. https://doi.org./10.1016/j.jchromb.2017.10.029.
21. Yu M, Cui FX, Jia HM, Zhou C, Yang Y, Zhang HW, Ding G, Zou ZM. Aberrant purine metabolism in allergic asthma revealed by plasma metabolomics. J Pharm Biomed Anal. 2016;120:181–9. .https://doi.org./10.1016/j.jpba.2015.12.018.
22. Ho WE, Xu YJ, Xu F, Cheng C, Peh HY, Tannenbaum SR, Wong WS, Ong CN. Metabolomics reveals altered metabolic pathways in experimental asthma. Am J Respir Cell Mol Biol. 2013;48(2):204–11. https://doi.org./10.1165/rcmb.2012-0246OC.
23. von Stechow L, Ruiz-Aracama A, van de Water B, Peijnenburg A, Danen E, Lommen A. Identification of cisplatin-regulated metabolic pathways in pluripotent stem cells. PLoS One. 2013;8(10):e76476. .https://doi.org./10.1371/journal.pone.0076476.
24. Zelena E, Dunn WB, Broadhurst D, Francis-McIntyre S, Carroll KM, Begley P, O'Hagan S, Knowles JD, Halsall A, Consortium H, Wilson ID, Kell DB. Development of a robust and repeatable UPLC-MS method for the long-term metabolomic study of human serum. Anal Chem. 2009;81(4):1357–64. .https://doi.org./10.1021/ac8019366.

25. Want EJ, Masson P, Michopoulos F, Wilson ID, Theodoridis G, Plumb RS, Shockcor J, Loftus N, Holmes E, Nicholson JK. Global metabolic profiling of animal and human tissues via UPLC-MS. Nat Protoc. 2013;8(1):17–32. https://doi.org./10.1038/nprot.2012.135.
26. Liu LW, Xing QQ, Zhao X, Tan M, Lu Y, Dong YM, Dai C, Zhang Y. Proteomic Analysis Provides Insights Into the Therapeutic Effect of GU-BEN-FANG-XIAO Decoction on a Persistent Asthmatic Mouse Model. Front Pharmacol. 2019;10:441. https://doi.org./10.3389/fphar.2019.00441.
27. Xing QQ, Liu LW, Zhao X, Lu Y, Dong YM, Liang ZQ. Serum proteomics analysis based on label-free revealed the protective effect of Chinese herbal formula Gu-Ben-Fang-Xiao. Biomed Pharmacother. 2019;119:109390. https://doi.org./10.1016/j.biopha.2019.109390.
28. Lim JCW, Goh FY, Sagineedu SR, Yong ACH, Sidik SM, Lajis NH, Wong WSF, Stanslas J. A semisynthetic diterpenoid lactone inhibits NF-κB signalling to ameliorate inflammation and airway hyperresponsiveness in a mouse asthma model. Toxicol Appl Pharmacol. 2016;302:10–22. https://doi.org./10.1016/j.taap.2016.04.004.
29. Kim MS, Radinger M, Gilfillan AM. The multiple roles of phosphoinositide 3-kinase in mast cell biology. Trends Immunol. 2008;29(10):493–501. https://doi.org./10.1016/j.it.2008.07.004.
30. Fruman DA, Bismuth G. Fine tuning the immune response with PI3K. Immunol. Rev. 2009;228(1):253–. 10.1111/j.1600-065X.2008.00750.x. 72.https://doi.org./.
31. Thomas M, Edwards MJ, Sawicka E, Duggan N, Hirsch E, Wymann MP, Owen C, Trifilieff A, Walker C, Westwick J, Finan P. Essential role of phosphoinositide 3-kinase gamma in eosinophil chemotaxis within acute pulmonary inflammation. Immunol. 2009;126(3):413–22. https://doi.org./10.1111/j.1365-2567.2008.02908.x.
32. Yang CM, Lee IT, Lin CC, Yang YL, Luo SF, Kou YR, Hsiao LD. Cigarette smoke extract induces COX-2 expression via a PKCalpha/c-Src/EGFR, PDGFR/PI3K/Akt/NF-kappaB pathway and p300 in tracheal smooth muscle cells. Am J Physiol Lung Cell Mol Physiol. 2009;297(5):L892–902. https://doi.org./10.1152/ajplung.00151.2009.
33. Kawahara K, Hohjoh H, Inazumi T, Tsuchiya S, Sugimoto Y. Prostagl and in E2-induced inflammation: Relevance of prostaglandin E receptors. Biochim Biophys Acta. 2015;1851(4):414–21. https://doi.org./10.1016/j.bbalip.2014.07.008.
34. Rogerio AP, Dora CL, Andrade EL, Chaves JS, Silva LF, Lemos-Senna E, Calixto JB. Anti-inflammatory effect of quercetin-loaded microemulsion in the airways allergic inflammatory model in mice. Pharmacol Res. 2010;61(4):288–97. https://doi.org./10.1016/j.phrs.2009.10.005.
35. Eltzschig HK. Adenosine: an old drug newly discovered. Anesthesiology. 2009;111(4):904–. 10.1097/ALN.0b013e3181b060f2. 15.https://doi.org./.
36. Xu X, Li J, Zhang Y, Zhang L. Arachidonic Acid 15-Lipoxygenase: Effects of Its Expression, Metabolites, and Genetic and Epigenetic Variations on Airway Inflammation. Allergy Asthma Immunol Res. 2021;13(5):684–96. https://doi.org./10.4168/aair.2021.13.5.684.
37. Basu S. Bioactive eicosanoids: Role of prostagl and in F2α and F2-isoprostanes in inflammation and oxidative stress related pathology. Mol Cells. 2010;30(5):383–91. https://doi.org./10.1007/s10059-

010-0157-1.

38. Kwang J, Baek, Jae, Youn, Cho P, Rosenthal, Laura E. Hypoxia potentiates allergen induction of HIF-1α, chemokines, airway inflammation, TGF-β1, and airway remodeling in a mouse model. Clin Immunol. 2013;147:27–37. https://doi.org./10.1016/j.clim.2013.02.004.
39. Tsuge K, Inazumi T, Shimamoto A, Sugimoto Y. Molecular mechanisms underlying prostaglandin E2-exacerbated inflammation and immune diseases. Int Immunol. 2019;31(9):597–606. https://doi.org./10.1093/intimm/dxz021.
40. Kang YP, Lee WJ, Hong JY, Lee SB, Park JH, Kim D, Park S, Park CS, Park SW, Kwon SW. Novel approach for analysis of bronchoalveolar lavage fluid (BALF) using HPLC-QTOF-MS-based lipidomics: lipid levels in asthmatics and corticosteroid-treated asthmatic patients. J Proteome Res. 2014;13(9):3919–29. .https://doi.org./10.1021/pr5002059.
41. Chang C, Guo ZG, He B, Yao WZ. Metabolic alterations in the sera of Chinese patients with mild persistent asthma: a GC-MS-based metabolomics analysis. Acta Pharmacol Sin. 2015;36(11):1356–66. .https://doi.org./10.1038/aps.2015.102.
42. Izquierdo-Garcia JL, Nin N, Ruiz-Cabello J, Rojas Y, de Paula M, Lopez-Cuenca S, Morales L, Martinez-Caro L, Fernandez-Segoviano P, Esteban A, Lorente JA. A metabolomic approach for diagnosis of experimental sepsis. Intensive Care Med. 2011;37(12):2023–32. .https://doi.org./10.1007/s00134-011-2359-1.
43. Yu M, Cui FX, Jia HM, Zhou C, Yang Y, Zhang HW, Ding G, Zou ZM. Aberrant purine metabolism in allergic asthma revealed by plasma metabolomics. J Pharm Biomed Anal. 2016;120:181–9. .https://doi.org./10.1016/j.jpba.2015.12.018.

Figures

Fig.1

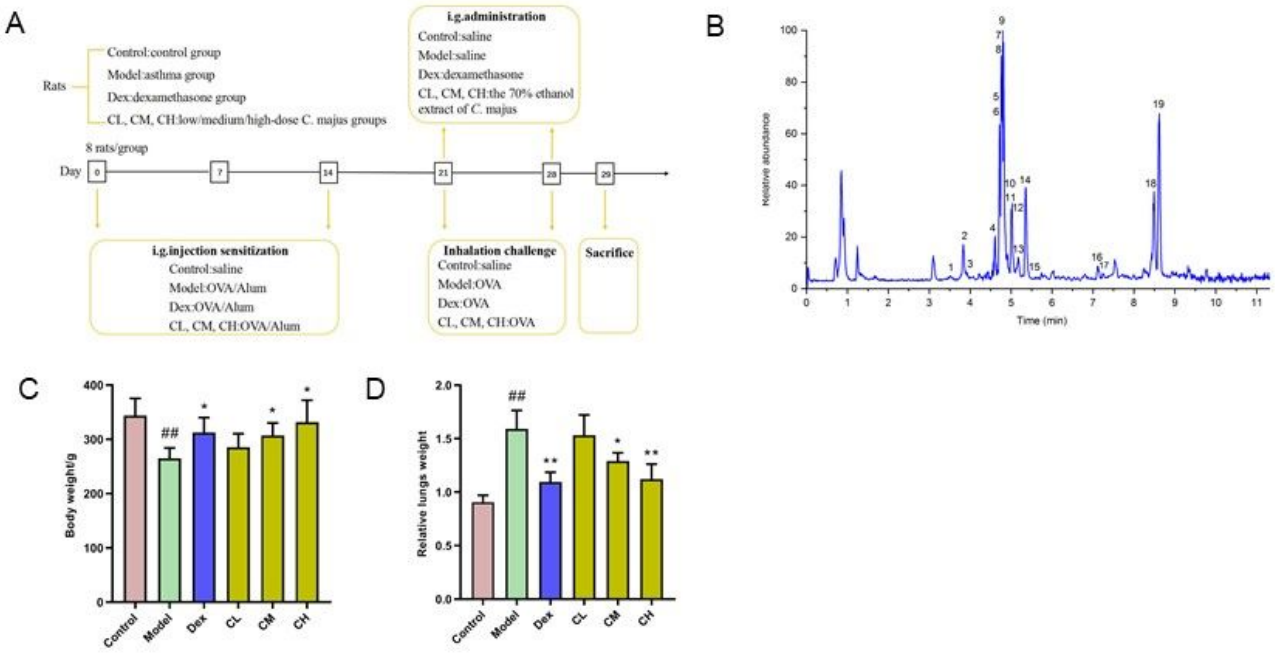

Figure 1

(A) Experimental scheme. (B) Total ion chromatograms (+) of *C.* majus extract. (C, D) Body weights and relative lung weights of diverse groups after administration.

Fig.2

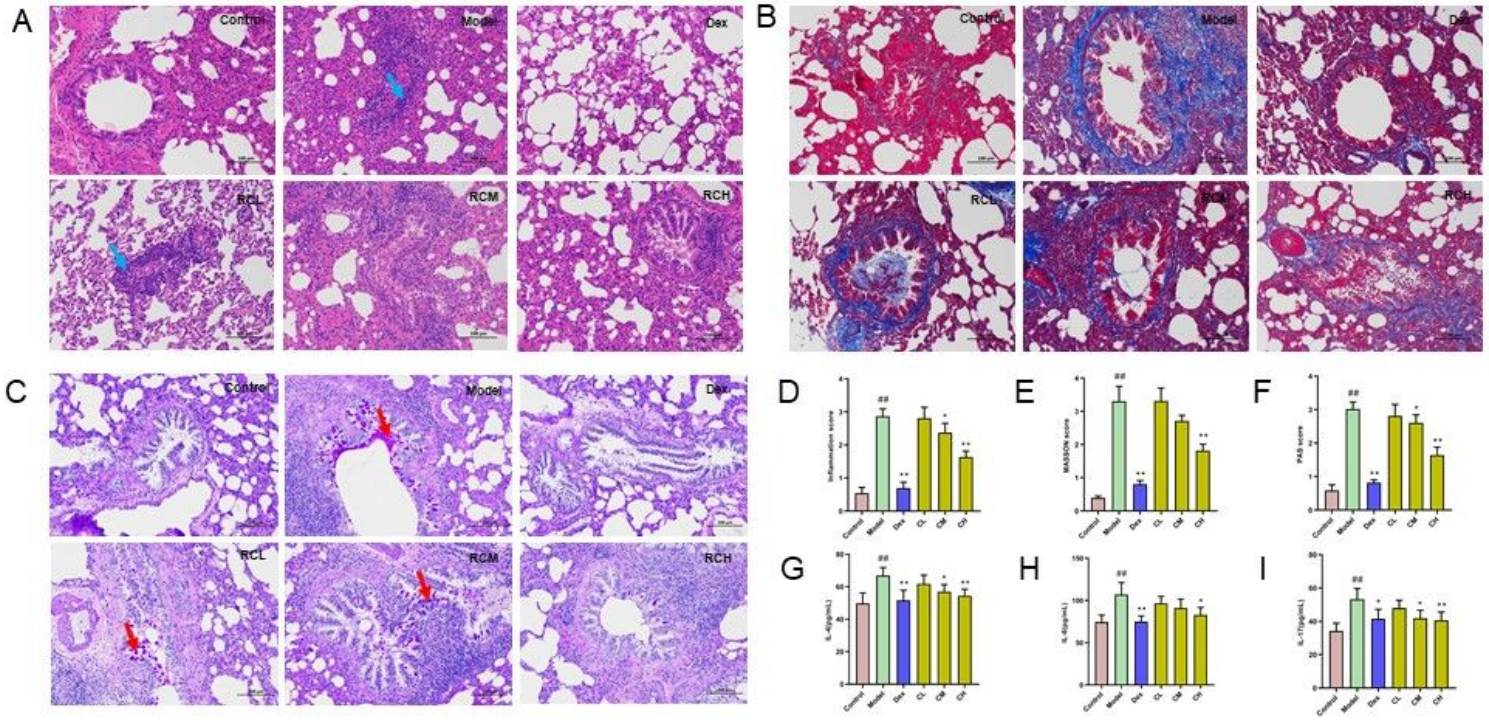

Figure 2

Pulmonary histopathology analysis. (A) H&E analysis (×200), blue arrows indicate inflammatory cell infiltration. (B) Masson analysis (×200). (C) PAS analysis of pulmonary sections (×200), red arrows indicate goblet cell proliferation. (D) inflammation score. (E) Masson score. (F) PAS score. The data are represented by mean ± SEM (n = 3). ##$p < 0.01$ versus Control group; *$p < 0.05$, **$p < 0.01$ versus Model group. (G-I) Inflammatory cytokinesassay. The data are represented by mean ± SEM (n = 8). ##$p < 0.01$ versus Control group; *$p < 0.05$, **$p < 0.01$ versus Model group.

Fig.3

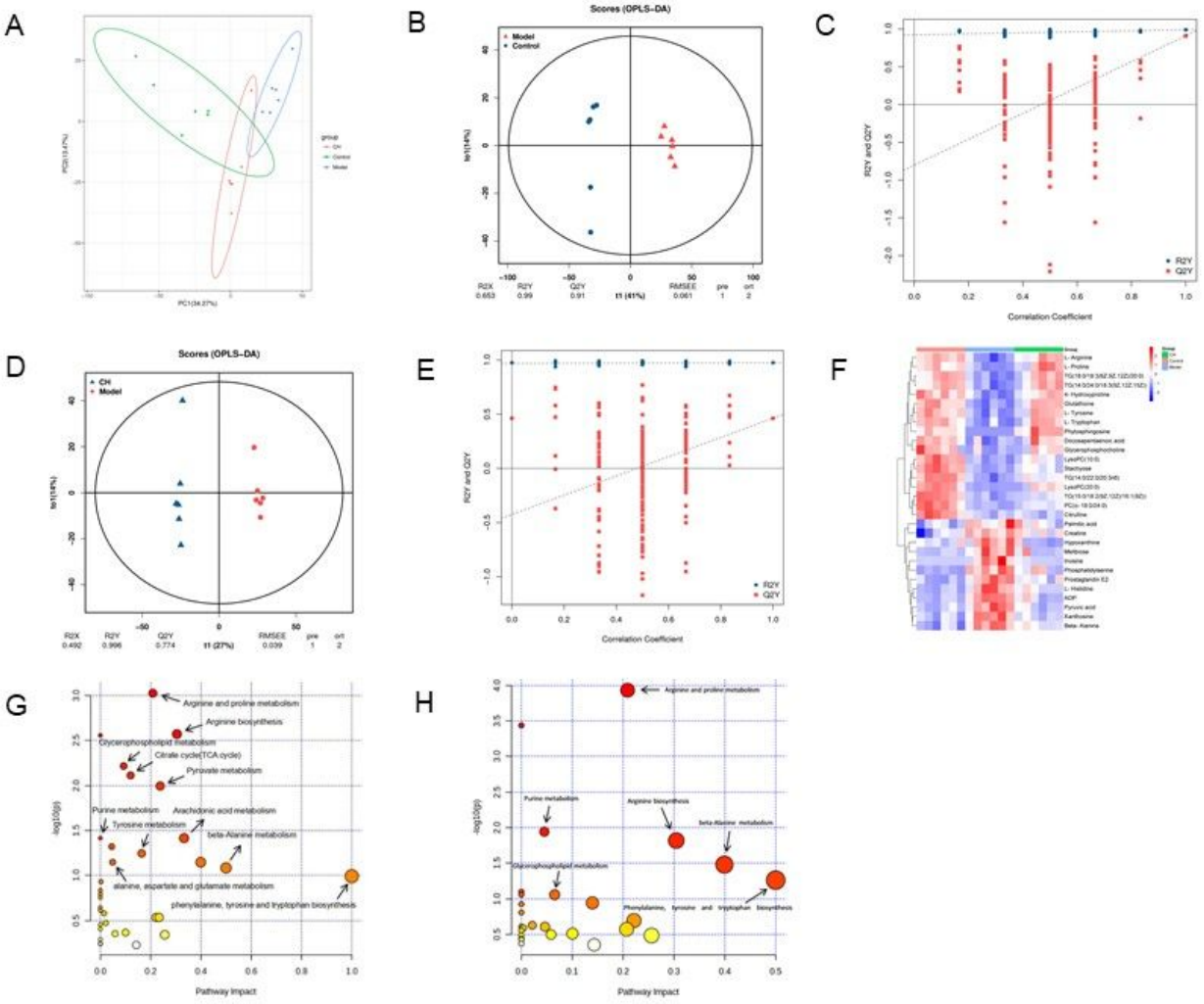

Figure 3

Metabolomic results. (A) PCA score plots. (B-E) OPLS-DA score plots. (F) Heatmap visualization for metabolic biomarkers in Control, Model and CH groups (n = 6). (G, H) Metabolic pathway analysis of Model-vs-Control group, Model-vs-Control group and CH-vs-Modelgroups.

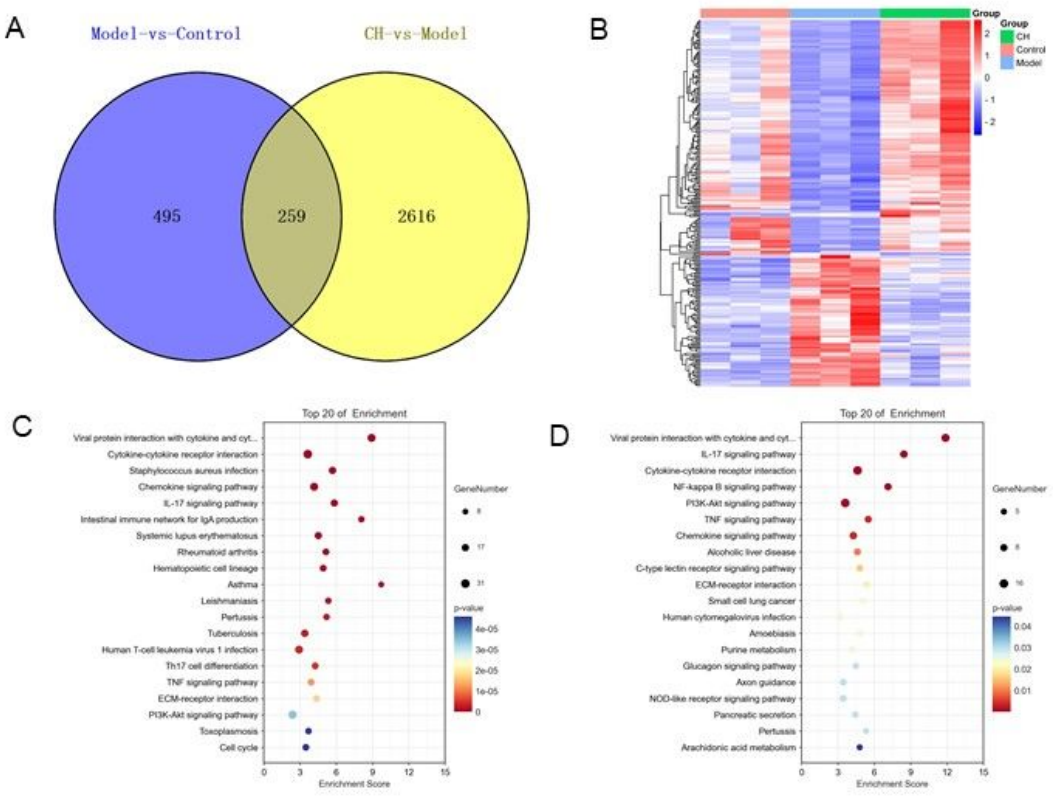

Figure 4

Transcriptomics results (n = 3). (A) Venn diagram showing DEGs in different groups. (B) Heatmap showing DEGs in Control, Model and CH groups. (C, D) KEGG pathway enrichment on DEGs-Bubble chart of Model-vs-Control group and Model-vs-Control and CH-vs-Model groups respectively.

Fig.5

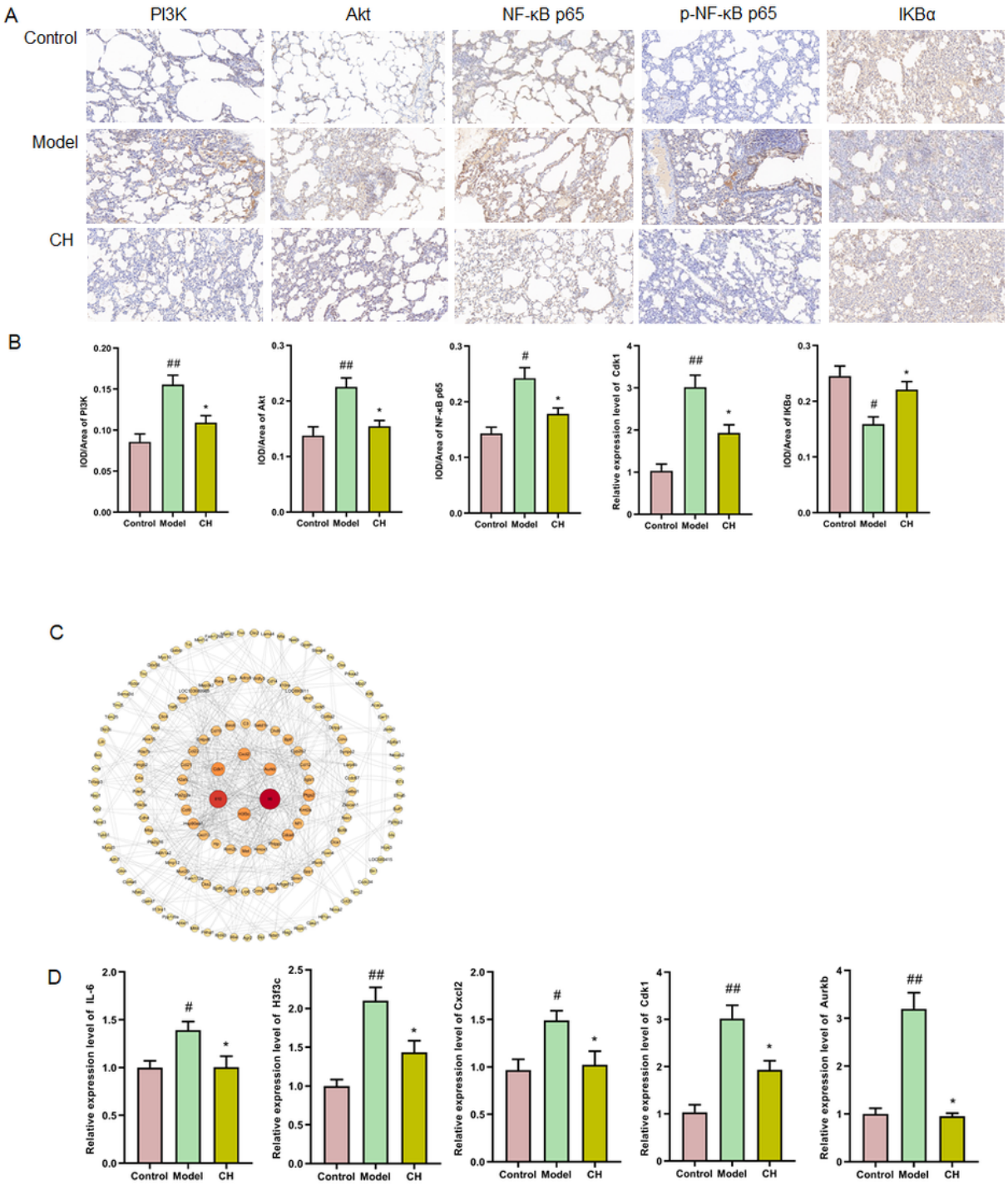

Figure 5

(A, B) IHC detection of PI3K, Akt, IKB-α, NF-κB p65, p-NF-κB p65 protein levels within rats lung tissues. The data is represented by mean ± SEM (n = 3). #$p < 0.05$, ##$p < 0.01$ versus Control group; *$p < 0.05$ versus Model group. (C) PPI networks regarding DEGs in Model-vs-Control and CH-vs-Model groups. (D) hub genes verification. Results are represented by mean ± SEM (n = 3). #$p < 0.05$, ##$p < 0.01$ versus Control group; *$p < 0.05$, **$p< 0.01$ versus Model group.

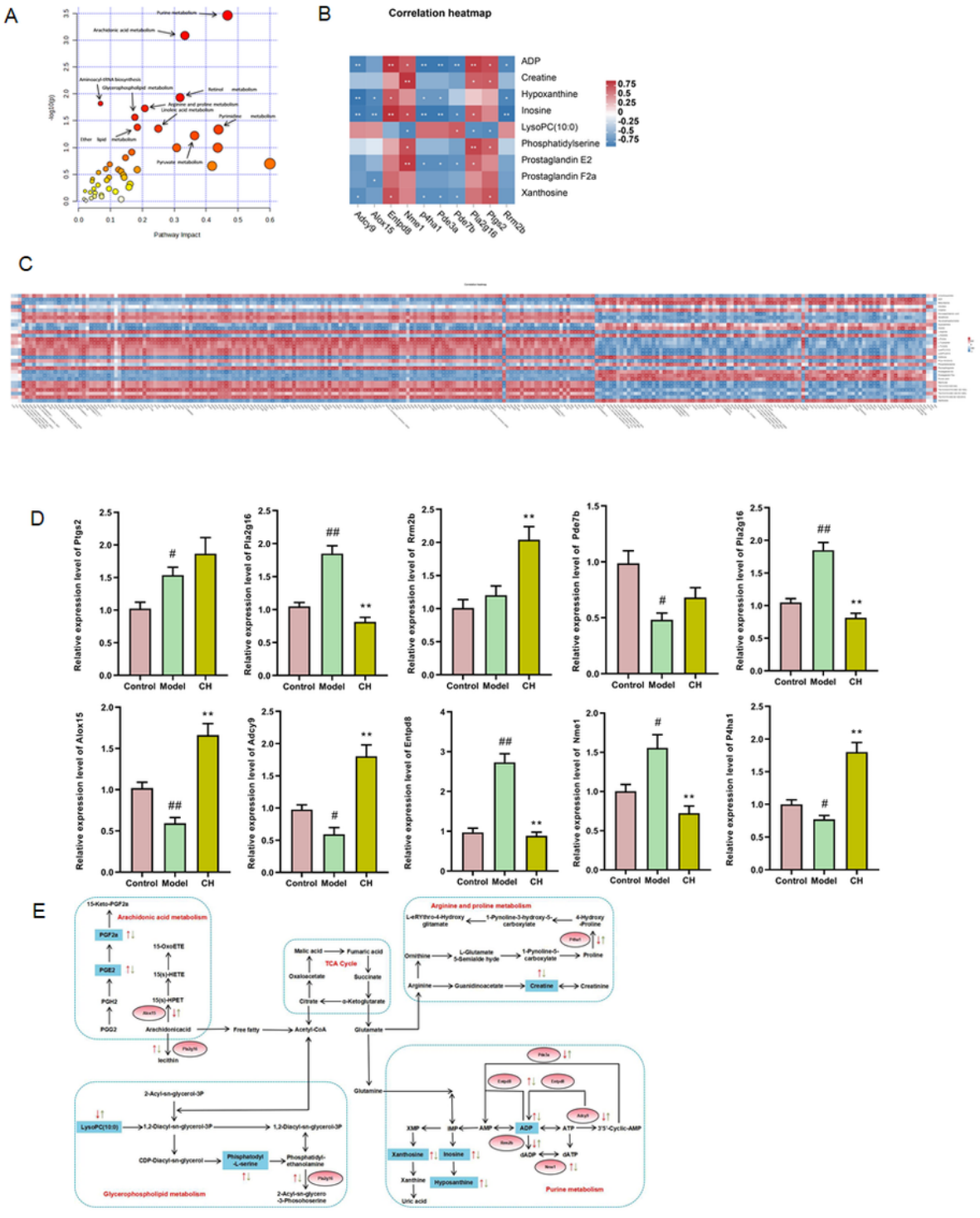

Figure 6

(A) Joint-Pathway analysis of Model-vs-Control and CH-vs-Modelgroups. (B, C) Correlation analysis between metabolic biomarkers and DEGs on the basis of spearman rank. (D) qRT-PCR validation of the 10 genes. Results are represented by mean ± SEM (n = 3). #$p < 0.05$, ##$p < 0.01$ versus Control group; *$p < 0.05$, **$p < 0.01$ versus Model group. (E) Changes in metabolites (blue squares) and differential genes (red circles) in the 4 metabolism on the basis of integrated analysis. The red arrow indicates the increase

or decrease of Model group relative to Control group. The green arrow reveals the increase or decrease of CH relative to Model group.

Supplementary Files

This is a list of supplementary files associated with this preprint. Click to download.

- Additionalfile1.xlsx
- Additionalfile2.xlsx
- Additionalfile3.xlsx